

Article

A Compact Circular Waveguide Directional Coupler for High-Order Mode Vacuum Electronic Devices

Tao Zhu ¹, Wenjie Fu ^{1,2,*} , Dun Lu ^{1,2} , Yibo Pan ¹, Chuannan Li ¹, Lin He ¹, Haoxuan Sun ¹ and Yang Yan ^{1,2}

¹ School of Electronic Science and Engineering, University of Electronic Science and Technology of China, Chengdu 610054, China; 202222021420@std.uestc.edu.cn (T.Z.); ludun@uestc.edu.cn (D.L.); yibopan@std.uestc.edu.cn (Y.P.); 202311021604@std.uestc.edu.cn (C.L.); 202122022105@std.uestc.edu.cn (L.H.); 202321021023@std.uestc.edu.cn (H.S.); yanyang@uestc.edu.cn (Y.Y.)

² Terahertz Science and Technology Key Laboratory of Sichuan Province, University of Electronic Science and Technology of China, Chengdu 610054, China

* Correspondence: fuwenjie@uestc.edu.cn

Abstract: In this paper, a compact circular waveguide directional coupler for high-order mode vacuum electronic devices is presented and investigated. To reduce the size, the primary and secondary waveguides of this coupler are connected in an orthogonal way by two coupling holes. Moreover, to improve the directivity and operating bandwidth, a method of loading adjustable metal stubs on the isolating port is proposed and introduced in design. A Ka-band TE₀₁-mode circular waveguide directional coupler was designed, and the structure parameters were optimized by electromagnetic simulation. To verify the design, a prototype sample was fabricated, assembled, and tested. The experimental results show good agreement with the simulations, and the directivity are improved by adjusting the metal stubs on the isolating port. In the experiment, a 26.7 dB directivity at 35 GHz was obtained, and the bandwidth of directivity above 20 dB was higher than 7 GHz, corresponding to a relative bandwidth higher than 20%. Meanwhile, the TE₀₁ mode maintained good transmission efficiency in this compact high-order mode directional coupler.

Keywords: vacuum electronic devices (VEDs); high-order mode; circular waveguide; directional coupler; Ka-band



Citation: Zhu, T.; Fu, W.; Lu, D.; Pan, Y.; Li, C.; He, L.; Sun, H.; Yan, Y. A Compact Circular Waveguide Directional Coupler for High-Order Mode Vacuum Electronic Devices. *Electronics* **2024**, *13*, 633. <https://doi.org/10.3390/electronics13030633>

Academic Editors: Syed Muzahir Abbas, Pradeep Lamichhane and Sohail Mumtaz

Received: 9 January 2024

Revised: 1 February 2024

Accepted: 1 February 2024

Published: 2 February 2024



Copyright: © 2024 by the authors. Licensee MDPI, Basel, Switzerland. This article is an open access article distributed under the terms and conditions of the Creative Commons Attribution (CC BY) license (<https://creativecommons.org/licenses/by/4.0/>).

1. Introduction

Vacuum electronic devices (VEDs) (e.g., Traveling-Wave Tube (TWT), Backward-Wave Oscillator (BWO), Klystron, and Gyrotron) are important high-power microwave radiation sources with extensive applications, which conventionally operate at fundamental electromagnetic (EM) modes [1–3]. As the operating frequency extends to millimeter-wave and terahertz bands, the power capability reduces as the size of the interaction circuits shrinks [4]. Therefore, in order to obtain sufficient power capability and high output power, operating in high-order mode is proposed and attempted in a large number of research works [5–12]. For example, the TM₀₁ mode is commonly employed for BWOs [7], the TE_{0n} mode or higher-order TE_{mn} mode is adopted for gyrotrons [8], and the TE_{n1} mode is usually utilized for the relativistic magnetrons [9]. In the research of VED system, real-time on-line monitoring of the output power is an important component. There are two common measurement methods, namely, the absorption-type measurement method represented by a calorimeter and the pass-by measurement method represented by a directional coupler. Compared with the former, the latter has been widely used in practical applications due to its excellent characteristics, such as on-line detection ability, high measurement accuracy, and strong anti-interference ability. However, although directional couplers have been studied for a long time and have been well developed, the research in the field of VEDs, where high-order modes are adopted as operating modes and high-order mode circular waveguides are adopted as transmission lines, is still quite limited.

Until recently, the mainstream research into directional couplers applied for the power monitoring of VEDs has mainly been focused on traditional aperture-type directional couplers [12–22], which are conventionally composed of a high-order mode circular waveguide (main waveguide) and a standard or non-standard rectangular waveguide (secondary waveguide), connected in a parallel or orthogonal way through two or more coupling apertures with various shapes. For structures where the primary and secondary waveguides are connected in a parallel arrangement, it is necessary to adjust the size, spacing, and number of the coupling holes to obtain excellent performance. However, since these variables are designed in the axial direction (the direction in which the electromagnetic wave propagates) of the coupler, it inevitably leads to a doubling of the axial length, which is usually more than ten times the wavelength [12–18], which makes the experimental operation inconvenient and reduces the compactness of the overall system. Another traditional structure is to connect the main and secondary waveguides of the coupler in an orthogonal way, which has the advantage of greatly reducing the axial length of the device. However, because the orthogonal connection mode limits the length of its coupling region, the disadvantage of this kind of structure is that its relative bandwidth is generally less than 10%, which means it can only work in a narrow band [21,22] so there are fewer studies on this structure.

In order to overcome the problems existing in the traditional structure (the contradiction between wide bandwidth and miniaturization), an improved double-hole high-order mode circular waveguide directional coupler is proposed in this work, adopting an orthogonal connection between the main and secondary waveguides, with three metal stubs loaded on the isolating port of the coupler, as shown in Figure 1.

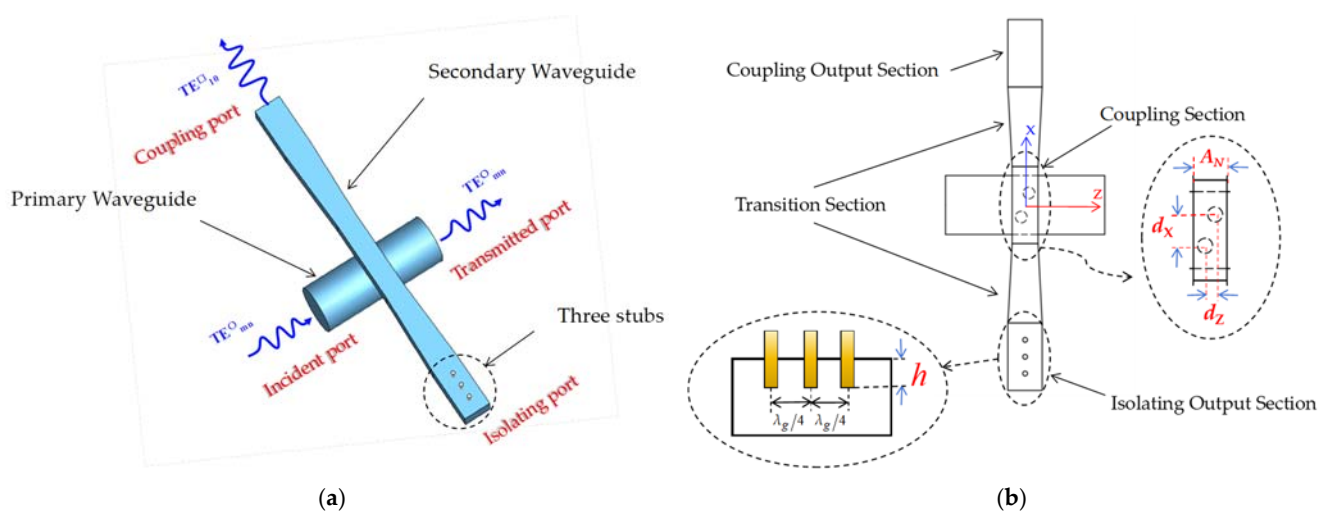


Figure 1. Structural diagram of the designed model. (a) The three-dimensional view; (b) the top view.

The structural diagram of the proposed high-order mode circular waveguide directional coupler is shown in Figure 1. The primary waveguide is circular waveguide, which transmits high-order mode waves. The secondary waveguide is rectangular waveguide, which transmits the fundamental TE_{10} mode wave. The primary and secondary waveguides are connected by two coupling holes that are symmetrically distributed around the original point in two dimensions (the X and Z axes). To obtain a high coupling efficiency, the size of the secondary waveguide is optimized based on the circular waveguide, and two transition segments are used to transition the non-standard waveguides to standard waveguides. Moreover, in order to overcome the shortcomings of the less than 10% bandwidth of the traditional orthogonal-type directional coupler, a novel method is proposed to adjust the directivity and output bandwidth of the coupler by inserting three metal stubs with insertion depths of h and spacing of $\lambda_g/4$ into a rectangular waveguide with lengths of λ_g (where λ_g is the operating wavelength of the waveguide) on the isolation port of the coupler.

To verify the proposed high-order mode circular waveguide directional coupler, a Ka-band TE₀₁ mode circular waveguide directional coupler was designed, fabricated and tested. The results present a good performance at 30.5–37.9 GHz and would be an acceptable approach in millimeter wave and terahertz wave applications. This article is organized as follows: Section 2 introduces the relevant theories and design process of the model. Section 3 introduces the simulation process of the model. Section 4 introduces the experimental process, and Section 5 draws the conclusion.

2. Principle and Design Model

Directional couplers are well-known passive four-port devices with a directional transmission function [16]. Figure 2 shows the schematic diagram of a common symmetrical double-hole directional coupler. To minimize the influence of the coupling holes on the transmission wave of the primary waveguide, the coupling between primary waveguide and secondary waveguide must be weak. Therefore, the amplitude of the wave transmitted from the input port to the pass-through port is generally regarded as constant [17]. Further, to simplify the study, the wall thickness of the waveguide is ignored. In the hypothesis that the shape and size of the two coupling holes are the same, their coupling degree is the same as well, denoted as a^\pm . At the same time, it is assumed that the phase constant of the incident wave in the primary waveguide is β_1 , the phase constant of the excited wave in the secondary waveguide is β_2 , and the two holes are located at $\pm d/2$ away from the symmetry center.

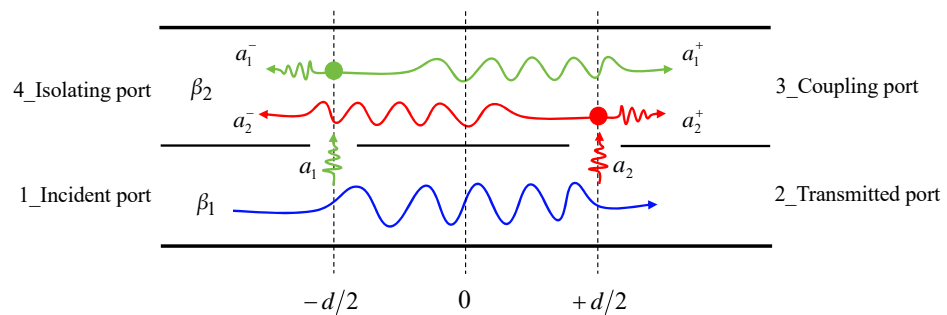


Figure 2. Schematic diagram of double-hole coupling.

The wave in the primary waveguide is transmitted from the incident port 1 to the transmitted port 2. During the propagation process, it arrives earlier at the first small hole (located at $-d/2$), at which a small amount of energy enters the transmitted ports 3 and 4, respectively, through the first hole. The relative field value of the reverse wave excited by the first hole in the secondary waveguide is denoted as a_1^- , while the relative field value of the forward wave excited by the first hole propagates to $+d/2$ after a distance of d in the secondary waveguide is denoted as $a_1^+ e^{-j\beta_2 d}$. And for the second hole, the incident wave first propagates to $+d/2$ after a distance of d in the primary waveguide, then the relative field value of the forward wave excited by the second hole in the secondary waveguide is $a_2^+ e^{-j\beta_1 d}$ at $+d/2$, and the reverse wave will propagate to $-d/2$ after a distance of d in the secondary waveguide, then the reverse wave obtained by the second hole in the secondary waveguide is $a_2^- e^{-j(\beta_1 + \beta_2)d}$. Since the size and shape of the holes are the same, their coupling degrees are also the same; that is, $a_1^\pm = a_2^\pm$.

Then the total forward wave in the secondary waveguide at $+d/2$ is

$$A^+ = a_1^+ e^{-j\beta_2 d} + a_2^+ e^{-j\beta_1 d} = 2a^+ e^{-j(\beta_1 + \beta_2)\frac{d}{2}} \cos[(\beta_1 + \beta_2)d/2], \quad (1)$$

and the total reverse wave in the sub-waveguide at $-d/2$ is

$$A^- = a_1^- + a_2^- e^{-j(\beta_1 + \beta_2)d} = 2a^- e^{-j(\beta_1 + \beta_2)\frac{d}{2}} \cos[(\beta_1 + \beta_2)d/2]. \quad (2)$$

At this time, their total relative amplitude is

$$A^\pm = |2a^\pm \cos \theta^\pm|, \tag{3}$$

where

$$\theta^\pm = \left| (\beta_1 \mp \beta_2) \frac{d}{2} \right|. \tag{4}$$

Obviously, when $\theta^+ = i\pi (i = 0, 1, 2, \dots)$, $|\cos \theta^+| = 1$, and the coupling of the two holes will be in phase superposition in the forward direction. Conversely, when $\theta^- = \left(i - \frac{1}{2}\right)\pi (i = 1, 2, \dots)$, $|\cos \theta^-| = 0$, and the coupling of the two holes will counteract in reverse, thus achieving the purpose of directional coupling.

In design, the major parameters that affect the performance of the coupler are the distances of the coupling holes (d_x and d_z in Figure 1b) and the wide-wall dimension (A_N) of the non-standard rectangular waveguide. Equation (4) can be further simplified as

$$\theta^\pm = \left| \left(\frac{2\pi}{\lambda_{g1}} \mp \frac{2\pi}{\lambda_{g2}} \right) \frac{d}{2} \right| = \left| \left(\frac{\lambda_{g1} \mp \lambda_{g2}}{\lambda_{g1}\lambda_{g2}} \right) \pi d \right| \tag{5}$$

where

$$\lambda_g = \lambda / \sqrt{1 - (\lambda/\lambda_c)^2} \tag{6}$$

The λ_c in the formula is the cutoff wavelength of the propagation mode in the waveguide. According to the size of the circular waveguide and the propagation mode number, λ_{g1} can be obtained. Further, the cutoff wavelength λ_{c2} of the non-standard rectangular waveguide in the coupling section can be obtained by $\lambda_{g1} = \lambda_{g2}$. Then, its wide-wall dimension can be obtained as $A_N = \lambda_{c2}/2$, and d_x can be obtained by means of the following equation:

$$\theta^- = \left(\frac{\lambda_{g1} + \lambda_{g2}}{\lambda_{g1}\lambda_{g2}} \right) \pi d_x = \left(i - \frac{1}{2} \right) \pi, i = 1, 2, 3 \dots \tag{7}$$

The double-hole directional couplers normally satisfy the above phase relationship only at one frequency point (usually the central frequency) [17], that is, they obtain satisfactory directivity only at this frequency point. When the operating frequency deviates from this point, its directivity rapidly declines, which leads to its working frequency band being very narrow, conventionally less than 10%. The traditional solution is to increase the number of coupling holes, which is suitable for conventional couplers with a parallel connection of the main and secondary waveguide due to the sufficient space; however, it is not suitable for the orthogonal one due to its limited space. In order to satisfy the design requirements of high-order mode VEDs for broad bandwidth, high transmission efficiency and high directivity, the length of the entire device increases with the increasing number of coupling holes, usually reaching more than ten wavelengths [12,18], which is very unfavorable to the pursuit of device miniaturization and system compactness. To solve this problem, we propose a method of loading an adjustable load at the isolating port, and adjustable metal stubs that adjust the isolation of directional couplers are introduced in this investigation.

It can be seen that as the working frequency deviates from the center frequency, the waves entering the secondary waveguide through the coupling holes no longer satisfy the structure designed by Equation (4). At this time, most of the reverse waves in the secondary waveguide flow into the isolating port and no longer counteract, which leads to the rapid decrease in the isolating degree, resulting in a sharp reduction in the directivity and effective bandwidth. In this regard, as long as we try to eliminate these reverse waves flowing into the isolating port, the isolating degree increases, and thus the bandwidth increases. A feasible solution is to introduce appropriate reflection in the isolating port,

which reflects part of the electromagnetic wave flowing into the port, which counteract the subsequent incoming waves, to realize the weakening of the incoming wave and the increase in the isolating degree. Thus, the three-stub impedance generator is introduced in this investigation. As described in Figure 1b, the three-stub impedance generator is constructed by three metal stubs that are inserted into the rectangular waveguide. A metal stub is usually a round metal rod that passes vertically across the wide side of a rectangular waveguide, acting as an inductor in the waveguide. Three metal stubs with the same spacing of $\lambda_g/4$ in a rectangular waveguide with a length of λ_g (where λ_g is the operating wavelength of the waveguide) construct an impedance tuner. Through adjusting the insert depth of the three stubs, the impedance characteristics of the waveguide with three stubs can be adjusted. According to the principle of stubs impedance matching mentioned in [23,24], when there are three metal stubs with the same spacing of $\lambda_g/4$ in a rectangular waveguide, the three-stub can theoretically obtain an impedance that completely covers the Smith chart, and it is widely used in a microwave system as an impedance matching system. In this investigation, by introducing the three-stub in the isolating port, additional reflection can be generated due to the impedance transformation, and the performance of the proposed directional coupler can be improved.

In this study, to simplify it, we use the three stubs together and set the insert depth of h to be the same each time. Synthesizing the above analysis, we apply it to the design of the directional coupler. Three metal stubs with $\lambda_g/4$ spacing are loaded at the isolating port acting as a standing wave generator, which cause a reflection on the isolating port, and the intensity of reflection can be controlled by controlling the insertion depth of the stubs to achieve the effect of adjusting the isolating degree.

3. Design and Simulation

To verify the proposed method of designing the high-order mode circular waveguide directional coupler, a Ka-band TE₀₁-mode circular waveguide directional coupler was designed. The radius of the primary waveguide is 6.1 mm, and the center operating frequency is 35 GHz (corresponding operating wavelength is $\lambda \approx 8.6$ mm). According to Equation (4), as the phase constant changes, the fluctuation of the coupling curve changes as well, while the phase constant β_2 of the secondary waveguide can be adjusted by adjusting the wide-wall dimension of the non-standard rectangular waveguide. Thus, to enlarge the operating bandwidth, a non-standard rectangular waveguide is adopted as the secondary waveguide, for which the wide-wall dimension is $A_N \approx 5$ mm. Following Equation (7), the d_x value of two holes is

$$d_x \approx (8.4i - 4.2) \text{ mm}, i = 1, 2, 3 \dots \quad (8)$$

Considering that the length of the coupling section cannot exceed the size of the main waveguide, the value of d_x is only desirable at $i = 1$, that is, $d_x = 4.2$ mm. The initial structural parameters of the designed directional coupler are shown in Table 1.

Table 1. Initial structural parameters of the designed directional coupler.

	Dimension
Primary waveguide	$R = 6.1 \text{ mm}, L = 33 \text{ mm}$
Standard rectangular waveguide (WR-28)	$a \times b = 7.112 \text{ mm} \times 3.556 \text{ mm}, L_s = 14 \text{ mm}$
Non-standard rectangular waveguide	$a \times b = 5 \text{ mm} \times 3.556 \text{ mm}, L_N = 22 \text{ mm}$
Radius of the coupling holes	$r = 1.2 \text{ mm}$
Thickness of the coupling holes	$t = 1.5 \text{ mm}$
Distances of the coupling holes	$d_x = 4.2 \text{ mm}, d_z = 0 \text{ mm}$
Length of the transition section	$L_t = 16.5 \text{ mm}$

In our investigation, the simulation software Computer Simulation Technology (CST) Microwave Studio (MWS) was adopted to optimize the design parameters of the double-

hole coupler. The models with and without loading metal stubs were both simulated and compared.

Figure 3a shows the simulation results with different d_z values at the same d_x and A_N . According to the simulation results, the directivity of the coupler increases obviously with the increase in d_z . In addition, it is noted that there is resonance around 33.2 GHz, which increases with the increase in d_z . Through analysis, the results show that this resonance is caused by the neighbor TE₃₁ mode. In this design, the radius of the primary circular waveguide is 6.1 mm, in which the cutoff frequency of the TE₀₁ mode is about 30 GHz, and the neighbor higher mode is TE₃₁ mode with a cutoff frequency of about 33 GHz. Because the primary waveguide boundary is discontinuous due to the existence of coupling holes, the TE₃₁ mode would be excited in the primary waveguide, which would reduce the performance of the directional coupler. To suppress the TE₃₁ mode excitation, different d_z , d_x and A_N values were simulated and analyzed, and the simulation results are shown in Figure 3b,c. According to the simulation results, d_x and d_z almost have the same effect, both which mainly affect the direction of the coupler, while A_N mainly affects the resonance, and the resonance increases significantly with the increase in A_N . Through optimizing A_N , the jump around 33 GHz could be sufficiently reduced. Figure 4 shows the S-parameters at $A_N = 5.4$ mm, $d_x = 4.2$ mm, $d_z = 1.6$ mm, and the E field distribution in the center of the primary circular waveguide at 32.9 GHz, 33.1 GHz, 33.3 GHz, and 33.5 GHz.

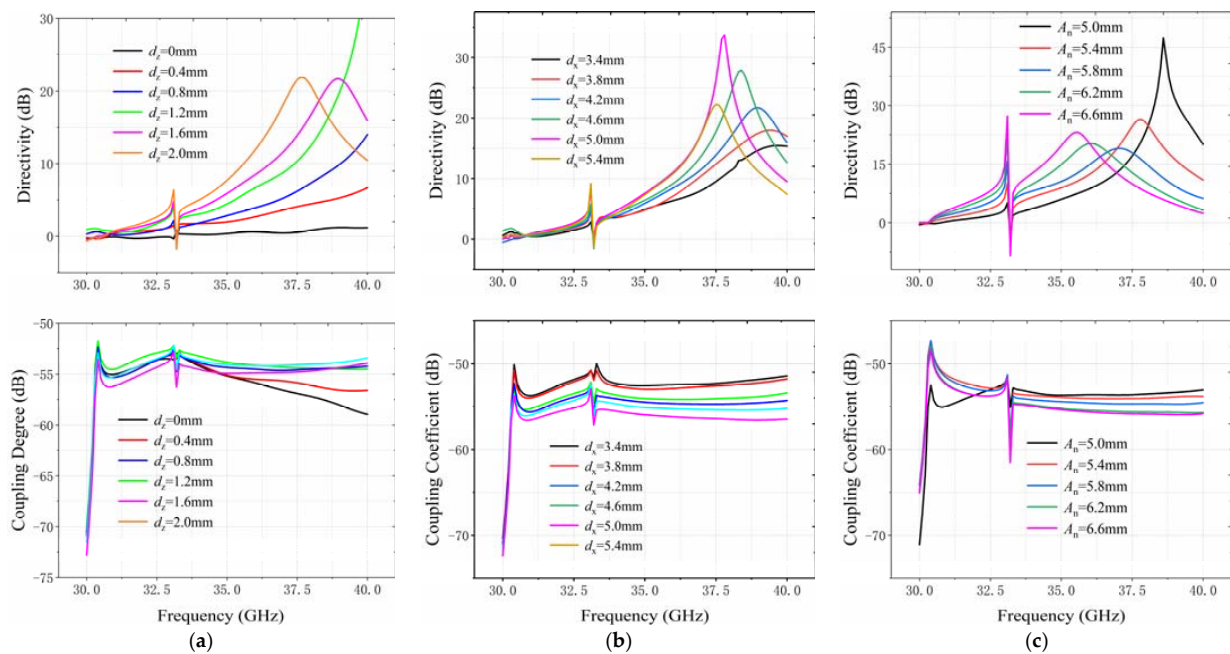


Figure 3. The coupling degree and directivity under (a) $A_N = 5$ mm, $d_x = 4.2$ mm with different d_z ; (b) $A_N = 5$ mm, $d_z = 1.6$ mm with different d_x ; (c) $d_z = 1.6$ mm, $d_x = 4.2$ mm with different A_N .

In order to obtain a higher directivity and as flat a coupling curve as possible, we set $d_x = 4.2$ mm, $d_z = 1.6$ mm, and $A_N = 5$ mm, based on which the function of metal stubs was further studied. To facilitate the study, we set the insertion depth of the three stubs to be the same, denoted as h . Figure 5 shows the coupling degree C , directivity D ($D = C - I$, where I is the isolating degree), and insertion loss (or transmission coefficient S21 of TE₀₁^o mode) of the coupler with different h . Moreover, the insertion loss is another important factor that should be considered in this design and optimization. Different from a conventionally fundamental mode waveguide directional coupler, in the high-order mode waveguide directional coupler, the boundary discontinuities caused by the coupling holes on the primary waveguide wall not only lead to reflections of the incident mode but also generate other spurious mode reflection and transmission. Thus, the insertion loss in this investigation only denotes the S21 of the input TE₀₁^o mode and output TE₀₁^o mode.

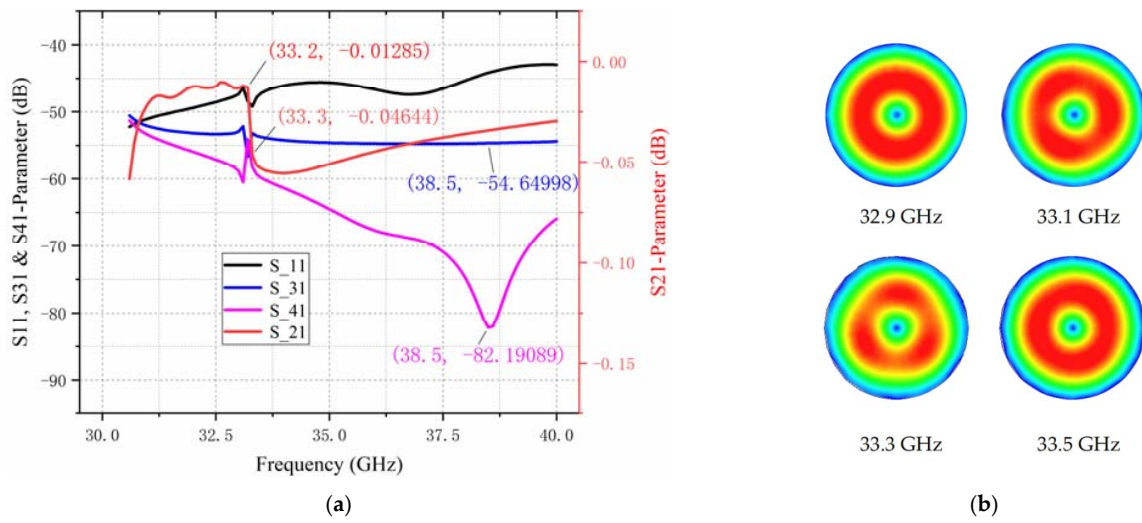


Figure 4. (a) Simulated S-Parameter at $A_N = 5.4$ mm, $d_x = 4.2$ mm, $d_z = 1.6$ mm; and (b) E-Field distribution at 32.9 GHz, 33.1 GHz, 33.3 GHz, 33.5 GHz.

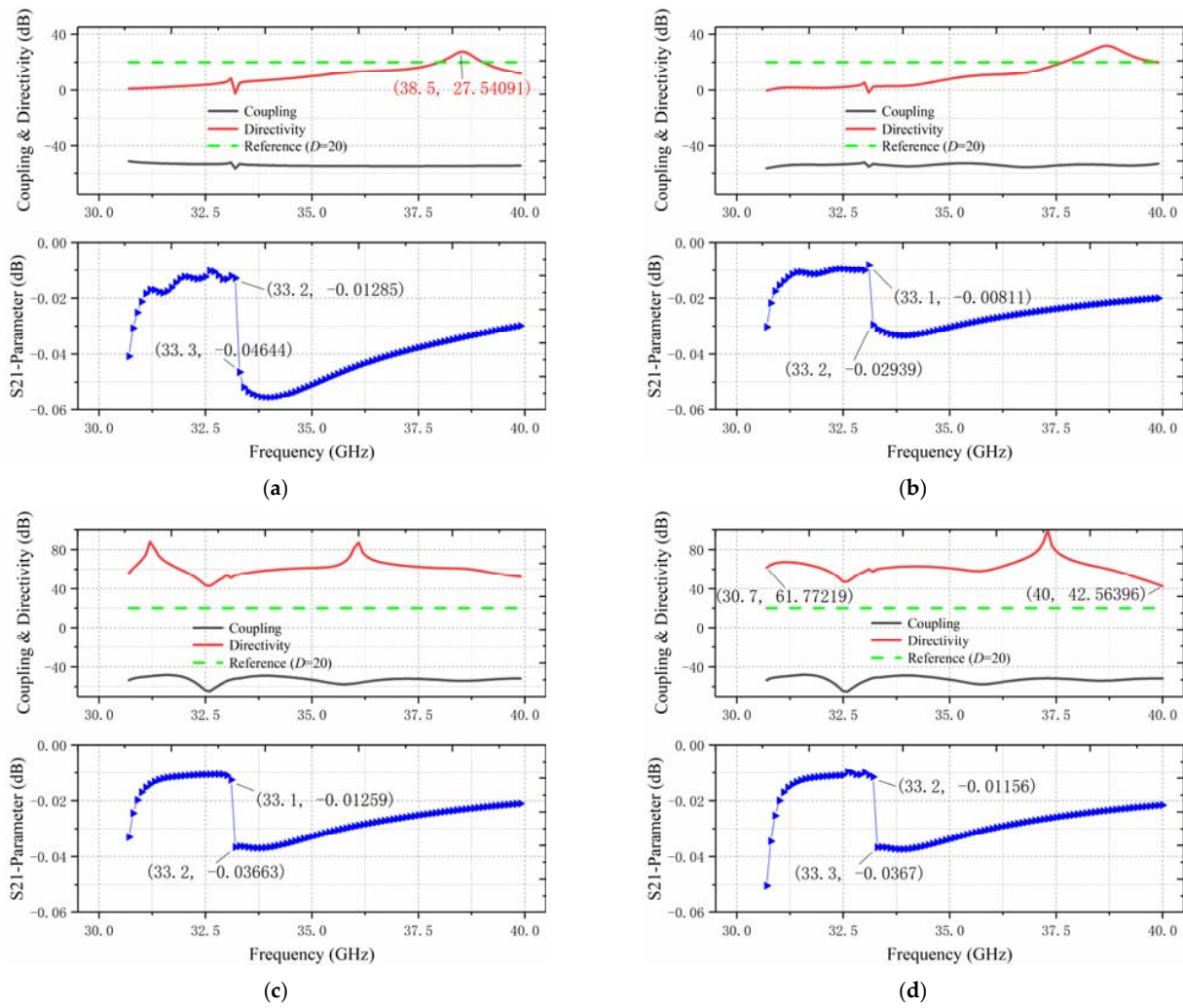


Figure 5. Simulation results under different insertion depths of stubs: (a) $h = 0$ mm; (b) $h = 1$ mm; (c) $h = 2$ mm; (d) $h = 3$ mm.

Figure 5 shows that when the insertion depths of the metal stubs were $h = 0$ mm, the total directivity of the coupler was low, the effective bandwidth was only 4.86%, and the

directivity at the center frequency of 35 GHz was less than 5 dB. When the insertion depth was 1 mm, the directivity and effective bandwidth of the coupler had a small increase. As the insertion depth increased to 3 mm, the overall directivity and effective bandwidth of the coupler greatly improved, with an effective frequency band of 9.3 GHz (from 30.7 GHz to 40 GHz), an effective bandwidth of 26.29% and a directivity of more than 40 dB at the center frequency of 35 GHz. Compared to couplers without loading stubs, the effective bandwidth increased about five times. In addition, it can be noted that the loading of stubs has little effect on the transmission efficiency (S21-Parameter) of the coupler, which reaches almost 100% over the entire frequency band.

However, it is worth noting that as the insertion depth of the metal stub increased, the original resonance was amplified, as shown in Figure 6. When the insertion depth of the metal stub became larger, the maximum fluctuation of the coupling curve was about 10 dB except for the resonance point.

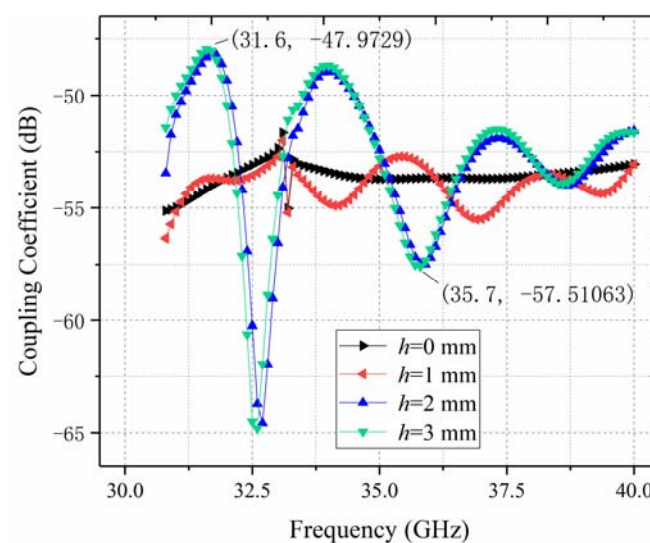


Figure 6. Fluctuation of the coupling curves with the changes in the insertion depth.

4. Experimental Verification

Based on the optimized parameters determined from the simulation results, a prototype coupler was fabricated, assembled, and tested. Figure 7 shows the test system and fabricated prototype sample. The total axial length of the manufactured sample was approximately 55 mm (about six times the operating wavelength), including a coupling section with a length of 33 mm and an input and output section, both with lengths of 11 mm.

In this experiment, an AV7632C (10 MHz–43.5 GHz) vector network analyzer (VNA) and two Ka-band TE_{10}° - TE_{01}° mode converters [5] were used. Due to a lack of circular waveguide calibration parts, the VNA was calibrated using WR28 waveguide calibration parts. A straight circular waveguide with the same length as the designed coupler was measured to deduct the loss of two TE_{10}° - TE_{01}° mode converters. The assembly steps of the entire test system were as follows. First of all, the VNA was connected to the waveguide–coaxial converters; the WR28 waveguide port will output TE_{10}^{\square} waves. Then, the waveguide–coaxial converters were connected to the TE_{10}° - TE_{01}° mode converters to convert the TE_{10}^{\square} mode into the required TE_{01}° mode. Finally, the TE_{10}° - TE_{01}° mode converters were connected to the fabricated sample and the matching-load was attached to the other two ports of the fabricated sample for testing. The detailed measurements are shown in Figure 8.

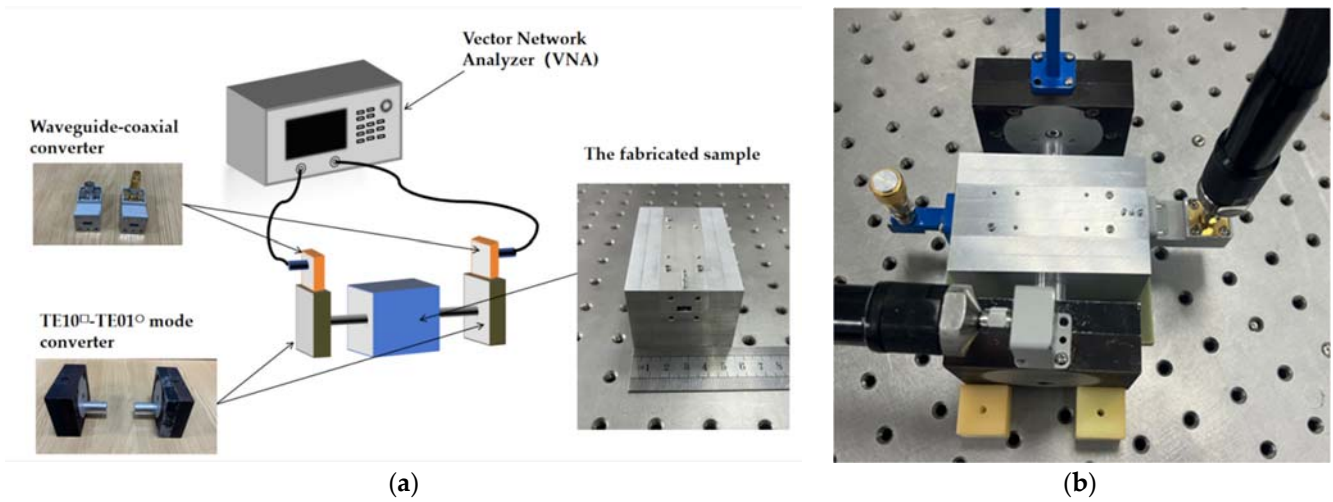


Figure 7. (a) The test system diagram; (b) the measurement of the fabricated sample.

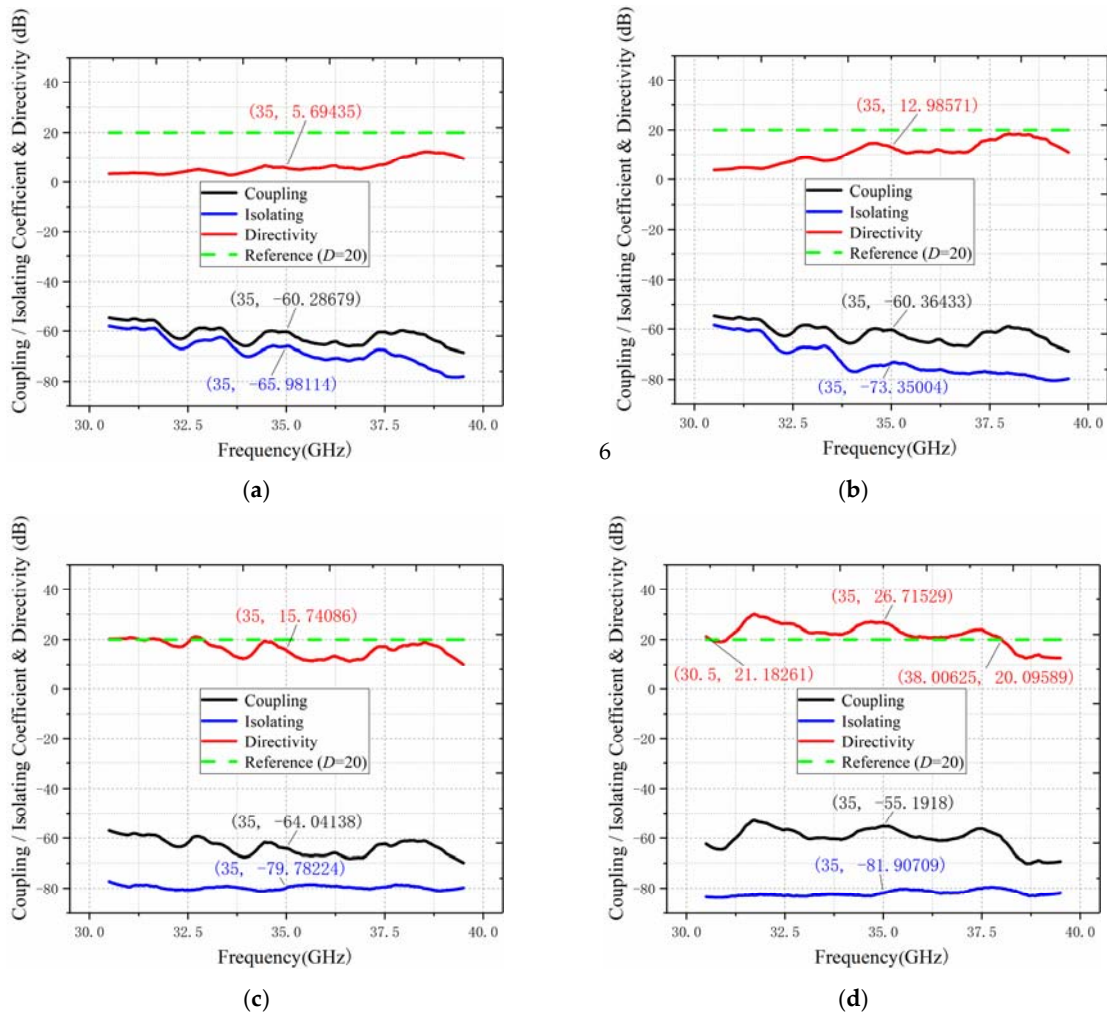


Figure 8. Measurements under different insertion depths of stubs: (a) $h = 0$ mm; (b) $h = 1$ mm; (c) $h = 2$ mm; (d) $h = 3$ mm.

As shown in Figure 8, the actual measurements were basically consistent with the simulation results. When the stub was not inserted or inserted at a lower depth, the directivity of the coupler was less than 20 dB. As the insertion depth of the stubs increased, both the directivity and the effective bandwidth of the coupler increased. When the

insertion depth of the stub was $h = 3$ mm, the directivity at the center frequency was about 26.7 dB, and the effective bandwidth in the entire frequency band was higher than 7 GHz, the corresponding relative bandwidth was higher than 20%.

Figure 9 shows the comparison between the simulated results and the measured results of the coupling curve and transmission coefficient (S21-Parameter) when $h = 3$ mm. From Figure 9, it can be seen that the measured insertion loss of the coupler at the center frequency is about -0.26 dB (the corresponding transmission efficiency is about 94.16%), indicating that the transmission efficiency of the coupler was high and the TE_{01} mode maintains high purity during transmission. It is worth noting that in the actual measurement, the fluctuation of the coupling curve was larger, and the maximum value was about 16.6 dB, which is larger than the simulation results and may be caused by machining and assembling errors.

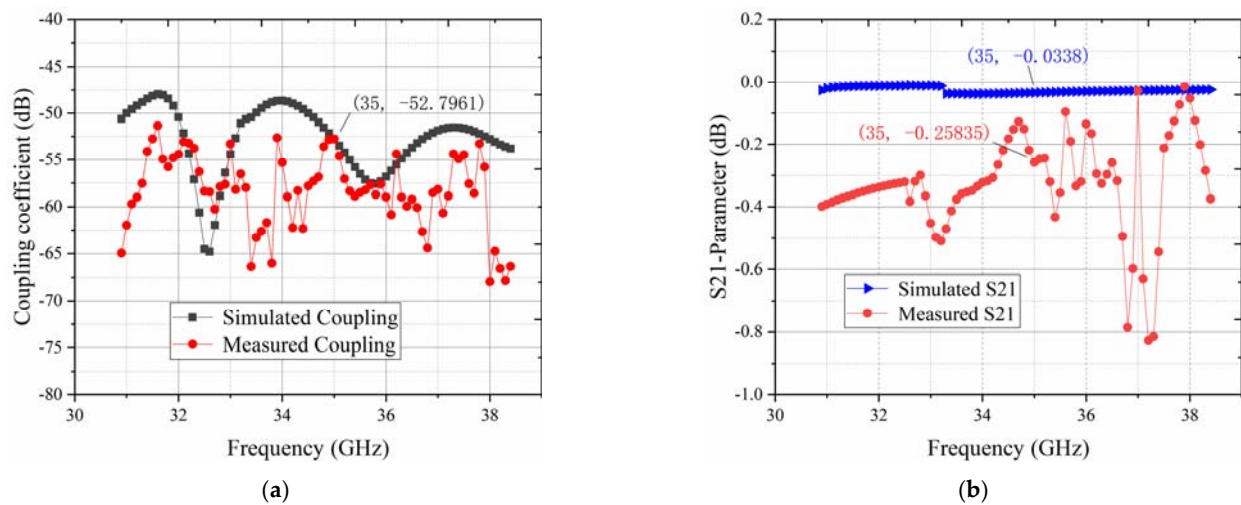


Figure 9. Simulated results and measured results at $h = 3$ mm: (a) coupling coefficient; (b) S21-Parameter.

Table 2 presents the measured performance comparison between this work and other configurations of aperture-type couplers, considering the operating bandwidth (OBW), effective bandwidth (BW, the band of $D > 20$ dB), directivity at center frequency (D), length of the coupling section (L), number of coupling holes (N), and the connection method of the primary and secondary waveguides (Con).

Table 2. Performance comparison of different aperture-type high-order mode circular-rectangular waveguide couplers.

	OBW (GHz)	OM	BW	D (dB)	L	N	Con
[10]	26.5–40	TE_{01}	-	>30	$16 \lambda_0$ *	32	Parallel
[19]	30–40	TE_{01}	$>20\%$	27	-	40	Parallel
	30–40	TE_{02}	$>20\%$	25	-	40	Parallel
[20]	8.8–10	TM_{01}	$<5\%$	23.7	$13 \lambda_0$ *	6	Parallel
[22]	9.8–10.2	TM_{01}	$<5\%$	25.6	$0.6 \lambda_0$ *	2	Orthogonal
This work	30.5–39.5	TE_{01}	$>20\%$	26.7	$3.85 \lambda_0$ *	2	Orthogonal

* λ_0 is the free space wavelength corresponding to the operating center frequency.

It can be seen from Table 2 that the structure in which the primary and secondary waveguides are connected in a parallel arrangement can obtain a larger bandwidth and directivity by adjusting the number of coupling holes, but it also makes the axial length of the device become particularly large, usually resulting in the total length being more than ten times its operating wavelength, which is very unfavorable to the operation of the

experiment and the miniaturization of the system. The orthogonal connection of the main and secondary waveguides can greatly reduce the axial length of the device. However, this connection mode limits the length of the coupling region, which means it is no longer suitable to increase the bandwidth and directivity by increasing the number of coupling holes. Therefore, the effective bandwidth of orthogonal-type structures is usually narrow and difficult to improve. In this work, large bandwidth and directivity can be obtained, while the length of the device can be greatly reduced.

5. Conclusions

In this paper, a novel compact circular waveguide directional coupler for high-order mode vacuum electronic devices is proposed, and the designed model and detailed method are presented. A Ka-band TE₀₁-mode circular waveguide directional coupler was designed according to this method, and a prototype sample was manufactured and tested. Both the simulation and experimental results show, through adjusting the metal stubs on the isolating port, that the performance of the directional coupler can be improved; meanwhile, the TE₀₁ mode maintains good transmission efficiency. In the experiments, 26.7 dB directivity at 35 GHz is achieved, and the bandwidth of directivity above 20 dB is higher than 7 GHz, corresponding to a relative bandwidth greater than 20%. This investigation mainly overcomes the contradiction between the broadband width output and miniaturization of traditional structures, which could be a desirable choice for the design of high-order mode directional couplers with broadband width, high directivity, and high compactness.

Author Contributions: Conceptualization, T.Z. and W.F.; methodology and investigation, T.Z. and D.L.; recourse, Y.P., C.L., L.H. and H.S.; writing—original draft preparation, T.Z.; writing—review and editing, W.F.; funding acquisition, W.F.; project administration, Y.Y. All authors have read and agreed to the published version of the manuscript.

Funding: This work was supported in part by the National Natural Science Foundation of China under Grant 62371105, 61971097, in part by Sichuan Science and Technology Program under Grant 2023YFH0028, and in part by the Guangxi Key Laboratory of Wireless Wideband Communication and Signal Processing under Grant GXKL06230201.

Data Availability Statement: The data presented in this study are available on request from the corresponding author.

Acknowledgments: The authors gratefully acknowledge Weirong Deng for their kind assistance with engineering design.

Conflicts of Interest: The authors declare no conflicts of interest.

References

1. Gilmour, A.S., Jr. *Principles of Klystrons, Traveling Wave Tubes, Magnetrons, Cross-Field Amplifiers, and Gyrotrons*; Artech House: Norwood, MA, USA, 2011.
2. Booske, J.H.; Dobbs, R.J. Vacuum Electronic High Power Terahertz Sources. *IEEE Trans. Terahertz Sci. Technol.* **2011**, *1*, 54–75. [[CrossRef](#)]
3. Granatstein, V.L.; Parker, R.K.; Armstrong, C.M. Vacuum electronics at the dawn of the twenty-first century. *Proc. IEEE* **1999**, *87*, 702–716. [[CrossRef](#)]
4. Li, X.; Wang, J. Analysis of electromagnetic modes excited in overmoded structure terahertz source. *Phys. Plasmas* **2013**, *8*, 083105. [[CrossRef](#)]
5. Han, M.; Fu, W.; Lu, D.; Zhang, C.; Hu, S.; Yan, Y. Quasi-optical Mode Converter Based on All-Dielectric Metamaterial for High-Order Mode Vacuum Electronics Devices. *IEEE Trans. Electron. Devices* **2023**, *70*, 2834–2839. [[CrossRef](#)]
6. Yang, T.; Guan, X.; Fu, W.; Lu, D.; Yuan, X.; Yan, Y. Investigation on 220 GHz Taper Cascaded Over-Mode Circular Waveguide TE_{0n} Mode Converter. *Electronics* **2021**, *10*, 103. [[CrossRef](#)]
7. Min, S.H.; Kwon, O. Design Study of GW-THz Wave Transmission without Mode Competition in an Oversized Relativistic Backward Wave Oscillator. *IEEE Trans. Plasma Sci.* **2017**, *45*, 610–622. [[CrossRef](#)]
8. Fu, W.; Guan, X.; Yan, Y. Generating High-Power Continuous-Frequency Tunable Sub-Terahertz Radiation from a Quasi-Optical Gyrotron with Confocal Waveguide. *IEEE Electron. Device Lett.* **2020**, *41*, 613–616. [[CrossRef](#)]

9. Liu, M.; Schamiloglu, E.; Jiang, W.; Fuks, M.; Liu, C. Investigation of the operating characteristics of a 12 stepped-cavity relativistic magnetron with axial extraction driven by an “F” transparent cathode using particle-in-cell simulations. *Phys. Plasmas* **2016**, *23*, 112109. [[CrossRef](#)]
10. Sun, M.; Xu, Y.; Li, Y.; Liu, Z.; Peng, T.; Luo, Y. Design and Test a Broadband Circular Waveguide Directional Coupler. In Proceedings of the 2018 International Conference on Microwave and Millimeter Wave Technology (ICMMT), Chengdu, China, 6–9 May 2018.
11. Wang, Z.; Wang, W.; Fang, H. A Compact and Broadband Directional Coupler for High-Power Radio Frequency Applications. *IEEE Microw. Wirel. Compon. Lett.* **2020**, *30*, 164–166. [[CrossRef](#)]
12. Wang, W.; Liu, G.; Jiang, W. Design and Measurement of a Broadband Compact TE₁₁ Mode Input Coupler for X-Band Gyrotron Traveling Wave Tube. *IEEE Trans. Microw. Theory Tech.* **2020**, *68*, 4554–4559. [[CrossRef](#)]
13. Zhang, Y.; Wang, Q.; Ding, J. A Cross-Guide Waveguide Directional Coupler with High Directivity and Broad Bandwidth. *IEEE Microw. Wirel. Compon. Lett.* **2013**, *23*, 581–583. [[CrossRef](#)]
14. Wang, X.; Zhao, P.; Yang, T.; Bi, K.; Tian, Z.; Xu, Z. A THz cross-guide Waveguide Directional Coupler with High Directivity. In Proceedings of the 2014 International Conference on Electronic Packaging Technology (ICEPT), Chengdu, China, 12–15 August 2014.
15. Labay, V.A.; Bornemann, J.; Rao, T.R. Design of Multilayered Substrate-Integrated Waveguide Cross-Slot Couplers. In Proceedings of the 2009 European Microwave Conference, Roma, Italy, 29 September–1 October 2009.
16. Zhang, B.; Niu, Z.; Wang, J. Four-hundred gigahertz broadband multi-branch waveguide coupler. *IET Microw. Antennas Propag.* **2020**, *14*, 1175–1179. [[CrossRef](#)]
17. Wang, W. *Microwave Engineering Technology*, 2nd ed.; National Defense Industry Press: Beijing, China, 2014; pp. 145–160.
18. Wang, W.; Liu, G.; Wei, J. Microwave Measurement of a Compact Circular TE₁₁ Mode Coupler Loaded with Ridges. *IEEE Trans. Electron. Devices* **2021**, *68*, 359–363.
19. Wu, Z.; Zhang, R.; Wang, M.; Liao, R.; Gao, H.; Huang, S.; Pu, Y.; Jiang, W.; Liu, G.; Wang, J.; et al. Circular TE_{0n} mode Content Analysis Technique for High-Power Gyro-TWT System. *IEEE Trans. Microw. Theory Tech.* **2022**, *70*, 1169–1177. [[CrossRef](#)]
20. Bai, Z.; Li, G.; Zhang, J.; Jin, Z. Design and Experiment of a Directional Coupler for X-band Long Pulse High Power Microwaves. *Rev. Sci. Instrum.* **2013**, *84*, 034701. [[CrossRef](#)] [[PubMed](#)]
21. Ma, J.; Zhong, W.; Zhang, H.; Zhang, C.; Xu, Z.; Sun, Z.; Chen, D.; Liu, Q.; Shen, Z. A Highly Directional Eight-hole Coupling Circular Waveguide Coupler. *Int. J. RF Microw. Comput.-Aid. Eng.* **2022**, *32*, e23208. [[CrossRef](#)]
22. He, C.; Zhang, W.; Ju, J.; Xu, L.; Cao, H. Design of Compact Directional Coupler for X-band Relativistic Triaxial Klystron Amplifier. *High Power Laser Part. Beams* **2023**, *35*, 60–65.
23. Bilik, V. Stub swapping in automatic three-stub impedance matching systems. In Proceedings of the 2013 Conference on Microwave Techniques (COMITE), Pardubice, Czech Republic, 17–18 April 2013.
24. Zhou, L.; Kuang, Y.; Li, S.; Fan, X.; Cheng, Q. Automatic Impedance Matching for Three-Stub Waveguide Tuner Based on Spacing Mapping. In Proceedings of the 2019 International Conference on Microwave and Millimeter Wave Technology (ICMMT), Guangzhou, China, 19–22 May 2019.

Disclaimer/Publisher’s Note: The statements, opinions and data contained in all publications are solely those of the individual author(s) and contributor(s) and not of MDPI and/or the editor(s). MDPI and/or the editor(s) disclaim responsibility for any injury to people or property resulting from any ideas, methods, instructions or products referred to in the content.